

# Interfacial structuration in a three-component polymer system

A. Aradian<sup>1,2\*</sup>, F. Saulnier<sup>1†</sup>, E. Raphaël<sup>1‡</sup> and P.-G. de Gennes<sup>1§</sup>

<sup>1</sup>Physique de la Matière Condensée, C.N.R.S. UMR 7125 & Fédération de Recherche MSC (FR 2438),

Collège de France, 11 place Marcelin Berthelot, 75231 Paris Cedex 05, France

<sup>2</sup> University of Edinburgh, School of Physics,

King's Buildings JCMB, Edinburgh EH9 3JZ, United Kingdom

May 22, 2019

## Abstract

We study theoretically the temporal evolution and the spatial structure of the interface between two polymer melts involving *three* different species (A, A\* and B). The chemical affinity between these polymer species, reflected by the pairwise Flory parameters  $\chi_{AB}$ ,  $\chi_{AA^*}$  and  $\chi_{A^*B}$ , are so chosen as to present strong contrasts: A and B are strongly attracted to each other ( $\chi_{AB} < 0$ ), A\* and B repel ( $\chi_{A^*B} > 0$ ), and A and A\* are fairly indifferent one to the other ( $\chi_{AA^*} \simeq 0$ ). We then show that, due to these contradictory tendencies, interesting properties arise during the evolution of the system: starting from an initial configuration where a melt containing a mixture of A and A\* is put in contact with a melt of pure B, the interface structures into several “compartments” of differing chemical compositions, and the spatial growth of the mixing layer takes place in a very asymmetric fashion. Such unusual behaviour might lead to interesting mechanical properties, and demonstrates on a specific case the potential richness of multi-component polymer interfaces for various applications.

## 1 Introduction and motivation

The phenomena taking place at the interfaces and surfaces of polymeric systems are obviously of high importance to many practical or industrial situations. As a result, they have been the

---

\*A.Aradian@ed.ac.uk

†Florent.Saulnier@college-de-france.fr

‡Elie.Raphael@college-de-france.fr

§PGG@curie.fr

focus of extensive study both experimentally and theoretically in the recent decades. Much progress has been made in the understanding of these phenomena as well as in the development of techniques to characterize them (see e.g. the general references 1–4).

## 1.1 Interfaces between polymer melts

One situation which has received much attention is that of two blocks of molten polymer put into (good) contact at a certain initial time: how does then the interface between these melts evolve, and how does the mixing between the melts occur, if any? or, more precisely, what is the final, equilibrium state reached by the system (i.e., given enough time, does it mix fully or only in a restricted region?), and with what kind of concentration profile? What is the dynamics leading to that final state, over which typical timescales? etc. It has been found,<sup>1,2</sup> due to the specific physics of polymer macromolecules, that their mixing is generally quite different from what is known in more conventional diffusive systems, like molecular gases. Once the two blocks are put into contact, the subsequent evolution will obviously generally depend on the various physico-chemical properties of the polymers facing each other (nature of microscopic interactions between monomers, chain length, topological structure, ...). It has been recognized however that, at least from a conceptual standpoint, the two most crucial parameters determining the fate of the system are the sign and magnitude of the product  $\chi N$ , where  $\chi$  is the Flory parameter,<sup>5</sup> related to the microscopic interactions between components, and  $N$  is the chain length. We will remind of the different possibilities for  $\chi N$  in section 2.

## 1.2 Multi-component interfaces

In order to facilitate the identification and modelling of the fundamental processes at work within polymer/polymer interfaces, past studies have for the most part, if not exclusively, focused on interfaces involving *two* species (for instance, one on each side of the interface) and sometimes only one species (interfaces between two identical melts). Certainly, the span of real situations is much wider, with a vast range of *multi-component interfaces*, and one is thus entitled to ask what is the structure and dynamics of an interface between two polymer *mixtures* involving more than two components.

As exemplified on the case studied in this article, such multi-component interfaces may have an interest of their own, as a means (for example) of obtaining *structured interfaces at the nanometer scale*: when two polymer mixtures are put into contact, and provided the contrast in relative miscibilities of the different components is adequate, a “multiple” interface may form; that is to say the interface will partition into several adjacent regions, each of different chemical composition. Such an interface could be frozen at a chosen time by quenching the sample,

and the mechanical properties presented by the resulting assembly might then possibly prove interesting.

Multi-species interfaces can also appear in the course of an interfacial reaction between two polymers: when the two blocks are put into contact, a reaction may start at the interface that delivers a (polymer) product whose miscibilities with each of the initial reactants are different; this three-species system is susceptible to lead to a multiple interface, whose dynamics is then coupled to that of the chemical reaction.

However, on purely combinatorial grounds, the diversity of all conceivable multi-component interfaces makes any general approach likely to be hopeless; thus delineating and focusing on a certain number of limiting situations may be useful. This is indeed the purpose of the present article: we will be considering one such “selected case” for a three-component interface, and will show that it exhibits a peculiar spatial structure and evolution through time, which we will fully analyze.

The article is organized as follows: in section 2, we start with a reminder on the standard theoretical results concerning two-component interfaces, as these will be used as basic tools for the rest of the paper. In section 3, we present the system that will be studied, and try to qualitatively explain the structure of the multiple interface which appears. In section 4, we write the equations governing the system and solve them, thus finding the lengthscales and concentration profiles which characterize the dynamics of our system (note that, if interested only in results, our reader can skip directly to section 4.3). Section 5 closes the article with some concluding remarks.

## 2 A reminder on two-component interfaces

We start here by a general reminder of the standard theories describing two-species interfaces. Denoting these species as A and B, we will cover interfaces occurring between an A-melt facing a B-melt, as well as between two mixed A-B blocks each made with different proportions of A and B. We will also mainly put the emphasis on the effect of varying the *Flory parameter*  $\chi_{AB}$  between A and B, with the assumption that both A and B have the *same* chain length  $N$ . Situations where  $N_A$  and  $N_B$  can differ (e.g. a melt of long chains facing a melt of short chains) will merely be hinted at, although also of interest (see, for instance, Ref. 6).

It is a remarkable point that the kinetics of formation of interfaces between chemically different polymers is controlled by thermodynamic as well as kinetic factors. To take into account the driving or slowing role played by energetic parameters in diffusion processes, it is much convenient to use Flory-Huggins’ derivation of the free energy (see eq. 6 for the expression

of the free energy  $f$  in this model, and also note 7): thinking in terms of a lattice model, the dimensionless *Flory parameter*  $\chi_{AB}$  characterizes the enthalpy of mixing at the molecular level, by comparing interactions between neighboring polymer segments of the same species (*i.e.*, association energy  $\epsilon_{AA}$  for two neighboring A segments,  $\epsilon_{BB}$  for two B segments) and interactions between different species in contact ( $\epsilon_{AB}$  for an A next to a B). If  $z$  denotes the coordination number in the lattice, we define

$$\chi_{AB} = \frac{z(2\epsilon_{AB} - \epsilon_{AA} - \epsilon_{BB})}{2kT} \quad (1)$$

In words,  $\chi_{AB}$  is the energy change, in units of the thermal energy  $kT$ , when a segment of A is taken from an environment of pure A and swapped with a segment of B from an environment of pure B. The Flory parameter  $\chi_{AB}$  can be positive or, much more rarely, negative. If the only interactions existing between A and B are van der Waals forces,  $\chi_{AB}$  shall be positive. Negative values of  $\chi_{AB}$  do appear in polymer couples displaying specific chemical interactions, such as hydrogen bonds. The three following subsections briefly discuss the different possible cases ( $\chi_{AB} > 0$ ,  $\chi_{AB} = 0$ ,  $\chi_{AB} < 0$ ).

## 2.1 Immiscible components: $\chi_{AB} > 0$

As stated above, in the absence of specific interactions or structural similarities, the Flory parameter is positive and usually ranges from  $10^{-3}$  to  $10^{-1}$ . This is by far the most usual situation for polymer pairs. For polymer pairs differing only by isotopic substitution (*e.g.*, when deuterium is substituted to hydrogen in the monomer structure), very small, positive values as low as  $\chi_{AB} \simeq 10^{-4}$  can be found.<sup>8</sup>

In this case of positive  $\chi_{AB}$ , the polymer pairs are *immiscible* for all but the lowest molecular weights: if  $N = N_A = N_B$  is the length of both polymers A and B, it can be shown that, for a Flory parameter  $\chi_{AB}$  greater than a critical value  $\chi_C = 2/N \ll 1$ , phase separation occurs and we end up at equilibrium with macroscopic regions of pure A and pure B, separated by a sharp interfacial layer: no macroscopic mixing occurs.

Let us precise the nature of this interface between the two coexisting phases by a simple scaling argument.<sup>9</sup> The characteristic width  $w$  of the interface can be estimated by a balance between the chain entropy (of order  $kT$  per chain), which tends to widen the interface, and the unfavorable enthalpy of mixing (of order  $\chi_{AB}$  per segment), which tends to narrow the interface: thus the typical length  $N_0$  of a loop of an A-chain penetrating a B-rich region is given by  $N_0 \chi_{AB} kT \sim kT$ , that is,  $N_0 \sim 1/\chi_{AB}$ . Because the loop has the form of a random statistical walk, this contour length corresponds to a (straight) penetration distance  $w \sim a\sqrt{N_{\max}}$  (where

$a$  is the monomer size). We finally find that the characteristic width of the interface is

$$w \sim \frac{a}{\sqrt{\chi_{AB}}} \quad (2)$$

This simple analysis is in accordance with the results obtained from a more rigorous description based on a square-gradient model of the interfacial free energy.<sup>9</sup> Note that the scaling analysis leading to this result is valid provided that  $\chi_{AB}N \gg 1$ : equation 2 then predicts the mixing region to be much smaller than the polymer coil size, and thus, at the macroscopic scale, the interface is to be considered as very sharp one, with a steep profile. This property of interfaces between immiscible melts will be used thereafter in our resolution (cf. Sec. 3.2).

## 2.2 Entropy-driven mixing: $\chi_{AB} = 0$

We now consider the case of a zero Flory parameter. Rigorously speaking, this situation arises when the two polymers put into contact are identical (same chemical structure). But it is also a useful approximation to describe mixing in systems with a very small  $\chi_{AB}$ , be it positive or negative (typically when  $|\chi_{AB}| \ll 1/N$ ).

Starting from a initial situation where two blocks of different composition are put into contact, the final, equilibrium state reached by the system is a homogeneous one (the initial interface has totally disappeared) with complete mixing of the polymer components. As there is no enthalpy gain associated with mixing species ( $\chi_{AB} = 0$ ), the evolution of the system is driven solely by gains in the translational entropy of the polymer chains.

The dynamics towards this final state can be complex, especially for entangled polymers where several regimes of non-Fickian diffusion successively appear. In these entangled polymers, the first stages of the interdiffusion process between melts of equal molecular weight have been described first within a scaling approach in Ref.11, and then detailed by different authors:<sup>12–15</sup> the chains are initially segregated on each side of the contact plane, with discontinuous concentration profiles abruptly dropping from unity to zero at the separation. Then, as the chains start interpenetrating to form a mixed layer, and because of the specific reptational dynamics of the polymer chains, this initial discontinuity survives, with a progressively resorbing amplitude, until disappearing when the reptation time  $T_{\text{rep}}$  is reached. The interface is then said to have “healed” completely. This feature stands in obvious contrast with conventional mixing where initial discontinuities are immediately smoothed out by the diffusion process.

For times greater than the reptation time ( $t > T_{\text{rep}}$ ), the interdiffusion dynamics becomes purely Fickian, and is described by the classical diffusion equation

$$\dot{\phi} = D_s \nabla^2 \phi \quad (3)$$

The diffusion coefficient  $D_s$ , known as the “self-diffusion” coefficient, is independent of concentration, and for long, entangled chains ( $N$  greater than the entanglement threshold  $N_e$ ), is equal to

$$D_s = \Lambda_0 \frac{N_e}{N^2} kT \quad (4)$$

where  $\Lambda_0$  is the monomeric mobility.

The use of eq 3 is valid only for facing melts with chains A and B of equal length (symmetric interfaces with  $N_A = N_B$ ). The case of *asymmetric* polymer junctions, between chemically identical melts of *different* molecular weights (typically a melt of short chains in contact with a melt of much longer chains) proves much more subtle. The evolution of the system (which also displays several temporal regimes) can essentially be understood as follows:<sup>16,17</sup> the long and less mobile chains behave like a gel which is progressively penetrated and swollen by the smaller species; but as the gel of long chains swells, it effectively drags the smaller chains within it. The global diffusion profile is thus rather complex and results from the microscopic diffusion of the small chains relative to the matrix of longer chains, combined with the global motion of this matrix. This global flow of the matrix, known as a “bulk-flow”,<sup>10</sup> is essential for a correct description of the system and will reappear in the next section devoted to enthalpy-driven species.

### 2.3 Enthalpy-driven mixing: $\chi_{AB} < 0$

Let us now consider the case of mixing between species driven by a gain in enthalpy, i.e., when  $\chi_{AB} < 0$ . A few dozens of A/B pairs with  $\chi_{AB} < 0$  have been reported, like PS/PVME (polystyrene/poly-vinylmethylether)<sup>18</sup> or PVC/PMMA (poly-vinylchloride)/poly-methylmethacrylate). Within the temperature range where  $\chi_{AB}$  remains negative, such polymer couples are fully miscible for all molecular weights.

The dynamics of “enthalpy-driven” mixing at interfaces between polymers has been the focus of many studies in the past 20 years, and its theoretical description has led to some controversy in the case where the system is *asymmetric*, e.g., when the mobility of the A and B chains are different (due to different chain lengths).

Based upon Onsager’s formalism of linear irreversible thermodynamics,<sup>19,20</sup> two main approaches were proposed.

The so-called “slow-mode” theory propounded by Brochard and co-workers<sup>21,22</sup>, assumes that the flux of species A is the opposite of the flux of B, i.e.,  $J_A = -J_B$ . In cases where the system is asymmetric, this hypothesis of cancellation of fluxes leads to a mutual diffusion coefficient dominated by the mobility of the *slowest* species—thus the name of theory.

On the other hand, Kramer and co-workers<sup>23</sup> explicitly introduce a third species in their model, which play the role of vacancies in the system and move about in order to allow the motion of A and B chains. Then the fluxes of the A and B components need not be equal anymore, and their difference  $J_A - J_B$  is compensated by a net flux of vacancies  $J_V$  across the cell.<sup>24</sup> It is furthermore postulated that the chemical potential of the vacancies is constant throughout the system, and this, contrarily to the theory of Brochard et al., leads to a “fast-mode” diffusion coefficient, i.e., dominated by the *fastest* species in asymmetric systems.

Experimental data indeed seem to validate the fast-mode theory.<sup>25–28</sup> However, to this day, the origin and physical interpretation of the vacancy flux in the model of Kramer et al. remains somewhat obscure. It is therefore most interesting to note that, in an amended version<sup>29</sup> of her previous model, Brochard has been able to retrieve the fast-mode predictions<sup>30</sup> without resorting to any flux of vacancies. Instead, Brochard’s corrected approach shows that, in addition to the individual diffusion fluxes of A and B, there exists a *global motion* involving both A and B which had not been taken into account earlier. The occurrence of such convective “bulk-flows” (as they are called), superimposed to pure diffusion, is indeed known as a common feature of asymmetric diffusive systems.<sup>10</sup> In the amended model of Brochard, each chain of polymer reptates and diffuses within a matrix composed of all the other chains; but this matrix *itself* is set into motion, due to the difference of mobility between the two diffusing species, thereby creating a bulk-flow in the system.

To describe the interdiffusion process of these two different polymers, one usually employs the so-called “mutual diffusion” coefficient  $D_M$ , which relates the *total* flux  $J_i$  of species  $i$  ( $i = A$  or  $B$ ) to the gradient of its volume fraction  $\phi_i$ :  $J_i = -D_M \nabla \phi_i$ . Let us denote  $\phi \equiv \phi_A = 1 - \phi_B$  the volume fraction of species A. In all the theoretical models mentioned above, the mutual diffusion coefficient can then be cast into the generic form:

$$D_M = \Lambda[\phi] \cdot \phi(1 - \phi) \cdot \frac{d^2 f}{d\phi^2} \quad (5)$$

where  $\Lambda[\phi]$  is a positive function of  $\phi$  (homogeneous to a mobility), which differs from model to model, and  $f$  is the classical Flory-Huggins free energy per site,<sup>7</sup> given by:

$$\frac{f}{k_B T} = \frac{\phi}{N_A} \log \phi + \frac{1 - \phi}{N_B} \log (1 - \phi) + \chi_{AB} \phi(1 - \phi) \quad (6)$$

In the rest of this article, we will only be concerned with the *symmetric* case, i.e., with polymer components of the same chain length ( $N_A = N_B \equiv N$ ) and the same monomeric mobility  $\Lambda_0$ . It should be pointed out that, in this case, the conceptual subtleties mentioned above do not intervene, and interdiffusion models do agree on the same expression of the diffusion coefficient. For long, entangled chains ( $N > N_e$ , the regime of interest to us), and using the same

notations as in eq. 4, one has simply  $\Lambda = \Lambda_0 N_e / N$ . From eq 5, the mutual diffusion coefficient then writes<sup>21-23</sup>

$$D_M = \Lambda_0 \frac{N_e}{N} kT \cdot \phi(1 - \phi) \cdot \left[ \frac{1}{\phi(1 - \phi)N} + 2|\chi_{AB}| \right] \quad (7)$$

A useful limit in practice is  $|\chi_{AB}|N \gg 1$ : as long as  $\phi$  and  $1 - \phi$  are larger than the (small) value  $\phi_c = 1/(2|\chi_{AB}|N)$ ,  $D_M$  can be approximated to

$$D_M = D_f \phi(1 - \phi) \quad \text{with} \quad D_f \equiv 2|\chi_{AB}|N D_s \quad (8)$$

( $D_s$  is the entropic, self-diffusion coefficient defined in eq 4).

Equation 8 shows that the diffusion coefficient in the enthalpy-driven mixing of polymers is strongly concentration-dependent. In particular, the vanishing of  $D_M$  for  $\phi = 0$  and  $\phi = 1$  leads to very unusual diffusion profiles when either of the polymer blocks in contact is initially pure in one of the mixture components.<sup>21</sup> When only one of the initial blocks is pure, the mixing width on the side of that block is *finite*, with a sharp edge; If both the initial blocks are pure, the width of the mixing region is finite on both sides, and, moreover, the diffusion profile within it is a *straight line*.

(Of course, as stated above, the simplified form 8 of  $D_M$  does not hold when  $\phi \rightarrow 0$  or  $\phi \rightarrow 1$ , and one has in fact to return to the full expression 7 for which  $D_M$  *does not* vanish at all... Thus, strictly speaking, the width of the mixing region is never exactly finite, and enthalpic diffusion profiles near  $\phi = 0$  and  $\phi = 1$  cross over to conventional, infinite “diffusion tails”. But this crossover occurs for  $\phi$  or  $1 - \phi$  of order  $\phi_c = 1/(2|\chi_{AB}|N)$ , and in the limit where  $|\chi_{AB}|N \gg 1$ ,  $\phi_c$  is so small that the diffusion tails contain a completely negligible mass of material.)

With this, we conclude our reminder on the different aspects of the theory of molten polymer interdiffusion, and come back to the problem of multi-species interfaces.

### 3 Description of the three-component system and qualitative approach

In this section, we present the specific system that we chose to study, and give some qualitative insight into the structure and dynamics that are expected to emerge. The next section will deal with this issues in a more rigorous way.

As explained in the introduction, the realm of multi-species system and their interfaces is a very vast one: our aim here is to explore one “model case” among these possibilities, involving three species, and where some interesting features do appear.

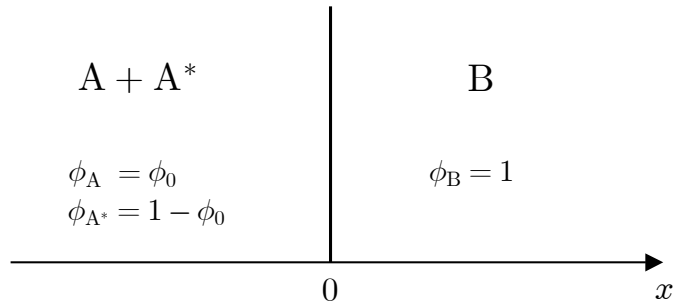


Figure 1: Initial situation of the three-species system. The left-hand block is made of a mixture of two polymers, A and A\*, with initial volume fractions  $\phi_A = \phi_0$  and  $\phi_{A^*} = 1 - \phi_0$ . The right-hand block contains only one species, called B, with initial volume fraction  $\phi_B = 1$ .

### 3.1 Description of the system and initial configuration

We now present the system that we will be concerned with in the rest of this article. The initial ( $t = 0$ ) situation is depicted in Figure 1: the system consists of two blocks of molten polymer which have just been put into contact. The surface of contact (the initial interface) between the blocks is assumed to be planar, and is located at position  $x = 0$  (the  $x$ -axis is drawn perpendicular to the surface). It is assumed that the problem is invariant in the two remaining spatial directions (parallel to the interface).

The system contains *three* polymer components which are initially distributed as follows: the left-hand block is made of a mixture of two polymers, A and A\*; the right-hand block is pure, i.e., contains only one species, which is called B. The important step (which is really defining our system) is now to specify the nature of the pairwise affinities between these three components. Our choice is the following: we assume that A and B are attracted to each other (through some specific interaction), and are thus miscible in all proportions; on the contrary, A\* and B strongly repel each other and thus have a tendency to form fully segregated phases; and, finally, A and A\* are fairly indifferent to each other (i.e., neither attracted or repelled, or not much). These features correspond to the following set of Flory parameters:

$$\chi_{AB} < 0, \quad \text{with} \quad |\chi_{AB}|N \gg 1 \quad (9)$$

$$\chi_{A^*B} > 0, \quad \text{with} \quad \chi_{A^*B}N \gg 1 \quad (10)$$

$$\chi_{AA^*} \simeq 0, \quad \text{with} \quad |\chi_{AA^*}|N \ll 1 \quad (11)$$

As we are mainly interested in the effect of the contrast in miscibility between the polymers, and not in chain length effects, it has been assumed above that all polymers have the same

polymerization index:

$$N_A = N_{A^*} = N_B = N. \quad (12)$$

A three-component system with such features as specified in eqs 9–11 would be quite difficult to realize experimentally, as the above requirements seem at first rather contradictory; they would certainly be achieved only through a fine tuning of the chemistry of the different polymers involved. One can imagine the following situation: A and B are rather different chemically, *but* are able to form H-bonds, which makes their global interaction very favorable. On the other hand,  $A^*$  is only a slight variant of A, modified just enough to inactivate the H-bonding; A and  $A^*$  are then fairly indifferent to each other, while between  $A^*$  and B, the “normal” (i.e., van der Waals) interactions become predominant again, and since their chemistry is quite different, make them immiscible. Another, powerful way to achieve such a system might also be through the use of *copolymers*.

Our choice of system is mainly guided here by the fact that it is one case that leads to the most interesting interfacial structure and dynamics. From the theoretical point of view, this interfacial problem is also original in the sense that, as will be seen shortly, it leads to simultaneous, coupled, entropy and enthalpy-driven diffusion processes.

### 3.2 Qualitative approach to the multiple interface structure

In this section, we present qualitative arguments explaining why, from the initial situation described in Figure 1, the interface between the two melts develops a “multiple” structure, i.e. displays multiple regions of different nature.

The situation of the interface as it is expected at time  $t > 0$  is depicted on Figure 2, and actually appears to be rather intuitive. As can be seen, the interface is divided in four main zones, labelled I–IV, which can be understood as follows. Immediately after the onset of contact, species A and B (which are attracted to each other) start to mix together, thus forming a growing, mixed layer (region II) around the initial position ( $x = 0$ ) of the surface of contact between the melts.

On the contrary,  $A^*$  is repelled by B, and thus recedes towards the left as region II broadens. Thus region I, which we define as the domain of coexistence of A and  $A^*$ , is progressively shrinking, with its right boundary moving towards the left. At the junction between region I (containing A and  $A^*$ ) and region II (containing A and B), there must be a region where *all* three species coexist (region IV). However, we expect this region IV to be of very small extension as compared to the others, since we know from section 2.1 that strongly immiscible polymers put into contact, like here  $A^*$  and B, tend to form a very sharp interface with a steep profile; hence, in the remaining of this article, we will neglect the thickness of region IV, and we will

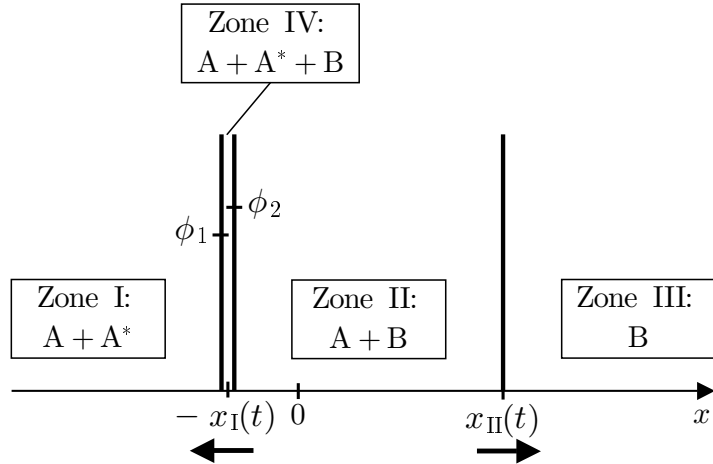


Figure 2: Multiple structure of the interface for  $t > 0$ . The arrows indicate the direction of motion of the regions' boundaries,  $x = -x_I(t)$  and  $x = x_{II}(t)$ . The quantities  $\phi_1$  and  $\phi_2$  indicate the values of the volume fraction in A at the boundaries of region IV.

not consider any detailed concentration profile within it. It must be emphasized however that region IV, albeit tiny, will act as a “filter” and thus will have a crucial effect on the dynamics of the system: all A chains which want to migrate from region I to II must cross region IV, so that the growth of region II will critically depend on what processes occurs within IV.

Finally, there is a last region, III, where B is alone: this comes from the fact that, as explained in Sec. 2.3, when one of the blocks in contact is initially pure (here,  $\phi_B = 1$  at  $t = 0$  for the right block), enthalpy-driven interdiffusion generates profiles with mixing only over a strictly finite width; thus, there is on the right side of region II a (time-dependent) location where the volume fraction of A reaches zero, and this is what defines the border with region III.

We also introduce in Figure 2 some notations that we will be using intensively in the next sections:  $x = -x_I(t)$  gives the position of region IV, and, in our limit where region IV is taken infinitesimally thin, plus or minus exponents ( $x = -x_I^\pm$ ) will respectively refer to the right and left boundaries of region IV;  $x = x_{II}(t)$  gives the position of the boundary between regions II and III; and  $\phi_1(t)$  and  $\phi_2(t)$  respectively denote the volume fractions of A just on the left and right of  $-x_I$ , i.e.,  $\phi_1 = \phi_A|_{x=-x_I^-}$  and  $\phi_2 = \phi_A|_{x=-x_I^+}$ .

After having presented an intuitive description of the interfacial structure and dynamics in our system, we will devote the next section to the establishment and resolution of the equations governing them.

## 4 Governing equations and results

In this section, we first establish the various equations governing the system (Sec. 4.1), and then solve them numerically (Sec. 4.2). The physical results of our computations are gathered and commented on in Sec. 4.3.

### 4.1 Governing equations

From now on,  $\phi_A$ , the volume fraction of A, will be simply denoted by  $\phi$ , i.e., we will use  $\phi(x, t) \equiv \phi_A(x, t)$ .

Let us start by enumerating our unknowns: these are the locations of the different regions' boundaries ( $x = -x_I$  and  $x = x_{II}$ ), the values of the volume fraction in A at  $x = -x_I^\pm$  ( $\phi_1$  and  $\phi_2$ ), and the time-dependent profile of  $\phi(x, t)$  within regions I and II (by definition,  $\phi = 0$  within region III). We will thus need a set of six independent equations to determine the solution of the system.

It should be noted that, from the knowledge of  $\phi$ , it is straightforward to retrieve the volume fractions of the other components of the system (using the total volume fraction condition  $\phi + \phi_{A^*} + \phi_B = 1$ ): in region I, where only A and  $A^*$  are present, one has  $\phi_{A^*} = 1 - \phi$  and  $\phi_B = 0$ ; in region II,  $\phi_B = 1 - \phi$  and  $\phi_{A^*} = 0$ ; finally, in region III,  $\phi_B = 1$  and  $\phi = \phi_A = 0$ .

We now establish the six independent equations which govern the dynamics of our system.

#### Diffusion equations

Our first equations simply describe the diffusive motion of polymer A. We must use two different equations, depending on the region considered within the multiple interface.

In region I, A chains diffuse inside an  $A+A^*$  mixture, with  $\chi_{AA^*} \simeq 0$  (eq 11); we are thus in a case of entropy-driven diffusion which is accounted for by equation 3,

$$\dot{\phi} - D_s \nabla^2 \phi = 0 \quad (\text{region I}) \quad (13)$$

and the initial and boundary conditions are as follows:

$$\phi(t = 0) = \phi_0; \quad \phi(x \rightarrow -\infty) = \phi_0, \quad \phi(x = -x_I^-) = \phi_1 \quad (14)$$

In eq 13, the entropic diffusion coefficient  $D_s$  is a constant parameter (see eq 4).

In region II, A chains diffuse into an  $A+B$  mixture, with  $\chi_{AB} < 0$  and  $|\chi_{AB}|N \gg 1$  (eq 9); we are there in the presence of an enthalpy-driven diffusion, for which the diffusion coefficient becomes concentration-dependent (see Sec. 2.3). Recalling eq 8, we have

$$D_f = 2|\chi_{AB}|ND_s \quad (D_f \gg D_s) \quad (15)$$

and the diffusion equation in region II can be written as

$$\dot{\phi} - D_f \nabla \cdot (\phi(1-\phi) \nabla \phi) = 0 \quad (\text{region II}) \quad (16)$$

with the initial and boundary conditions

$$\phi(t=0) = 0; \quad \phi(x=-x_I^+) = \phi_2, \quad \phi(x \rightarrow +\infty) = 0 \quad (17)$$

(see note<sup>31</sup>).

### Equation of motion for $x_{II}(t)$

Apart from the two diffusion equations 13 and 16, a third equation can be written, which relates to the motion of  $x_{II}(t)$ . By definition,  $x = x_{II}(t)$  denotes, for any time  $t$ , the moving point where the concentration profile  $\phi$  reaches zero (and beyond which only polymer B is present). As shown in the Appendix to this article, this very definition implies that the *velocity*  $\dot{x}_{II}$  of this point is related to the gradient of  $\phi$  on its left as follows:

$$\dot{x}_{II} = -D_f \nabla \phi|_{x=x_{II}^-} \quad (18)$$

### Conservation of the A and B species

We must naturally also take into account equations that ensure the conservation of the different polymer components in the system.

It is shown in the Appendix that the conservation equation for species A leads to the following relation between the velocity  $\dot{x}_I$  of the interface of regions I and II, and the volume fraction  $\phi_1$  of A and the gradient  $\nabla \phi|_{x=-x_I^-}$  on the left side of it:

$$\dot{x}_I = -\frac{1}{1-\phi_1} \cdot D_s \nabla \phi|_{x=-x_I^-} \quad (19)$$

The conservation of the B species, on the other hand, gives a relation between the same velocity  $\dot{x}_I$ , and the volume fraction and gradient on the *right* side of this interface:

$$\dot{x}_I = -\phi_2 \cdot D_f \nabla \phi|_{x=-x_I^+} \quad (20)$$

Note that the conservation of the third species,  $A^*$ , follows automatically from the conservation of the two others, through the relation between volume fractions  $\phi + \phi_{A^*} + \phi_B = 1$ , and thus does not bring us a new equation.

### An equilibrium relation between $\phi_1$ and $\phi_2$

At this point, we have written down five independent relations; as there are six unknowns, there must be a last physical constraint determining the dynamics of the system. We have so far totally ignored region IV (see Figure 2), where the three species A, A\* and B coexist. As stated earlier, this is because this region is expected to be of very limited extension, and, as such, has rightfully been discarded, e.g., from the A and B conservation equations discussed above. However, despite being negligible in mass, region IV must clearly play an essential role regarding the dynamics, since all the A material that diffuses from region I to region II has to transit through it.

Describing precisely the interdependent diffusive process at work within the three-body region IV—solving the “inner problem”, in the terms of boundary-layer theory—would undoubtedly represent a complex task and require a study of its own. We rather propose to bypass this difficulty, as we in fact only need very limited information for our purpose: we are only interested in the effect of region IV on the outer dynamics, not in internal details. We will here assume that region IV is always at *equilibrium*, i.e., that the concentration profile of each species within that region always adopts an equilibrium shape which satisfies the condition of *uniform chemical potential* for that species.

The physical origin of our assumption is that, given the small dimensions of region IV, material within it needs only to rearrange only over small distances to reach equilibrium; as a consequence, the equilibration time of region IV is negligibly small as compared to the timescale of the dynamics in the outer regions. We can thereby assume that the evolution outside region IV is an adiabatic process to which region IV is always able to instantaneously adapt to by finding the appropriate equilibrium state.

The last equation looked for should thus reflect this quasi-static behaviour of region IV, by stating that the chemical potential  $\mu_A$  of A is uniform across it, and in particular, that it has the same value at both ends of the region:

$$\mu_A(-x_I^-) = \mu_A(-x_I^+) \quad (21)$$

As shown in the Appendix, once the expressions of the chemical potentials are written out, this equality yields our last governing equation as a relation between the volume fractions  $\phi_1$  and  $\phi_2$  at the borders of region IV:

$$\phi_1 = \phi_2 \exp[-|\chi_{AB}|N(1 - \phi_2)^2] \quad (22)$$

We are now in possession of six independent equations which govern the dynamics in our system, and can proceed to solve them.

## 4.2 Technical resolution

We now present the procedure followed to solve the set of governing equations derived in the previous section (eqs 13, 16, 18, 20, 19, 22). We will here focus on the technical aspects of the resolution itself, while, for the sake of readability, we have grouped together the presentation of the results obtained and of their physical content in the next section (Sec.4.3).

The major difficulty attached to the interdiffusion problem as defined by this set of equations is that it involves two *moving boundaries*,  $x = -x_I(t)$  and  $x = x_{II}(t)$ . The resolution of moving boundary problems is generally much less straightforward than a conventional diffusion problem; we will here follow the solution scheme described in Crank.<sup>10</sup>

Our problem falls into the so-called “Class A” category,<sup>10</sup> characterized by the fact that the motion of the moving boundaries is directly due to the transfer of diffusing substances across them. (This is indeed the meaning of the conservation equations 36 and 38 in the Appendix). It is then possible to show that, in a generic fashion, the solution will have the following properties:<sup>10</sup>

- (i) The concentration of the diffusing species at the moving boundaries is constant, i.e.,  $\phi_1$  and  $\phi_2$  are *independent of time*.
- (ii) The motion of the moving boundaries is *diffusive*, i.e.  $x_I(t) \sim (D_s t)^{1/2}$  and  $x_{II}(t) \sim (D_f t)^{1/2}$ .

We build the solution to our problem with the help of these useful results. In accordance with property (ii) above, we introduce the new quantities  $a$  and  $b$  defined by:

$$x_I(t) = 2a (D_s t)^{1/2} \quad (23)$$

$$x_{II}(t) = 2b (D_f t)^{1/2} \quad (24)$$

The numerical value of these two quantities will have to be determined as a result of our resolution. We also define

$$\epsilon = \frac{D_s}{D_f} = \frac{1}{2|\chi_{AB}|N} \ll 1 \quad (25)$$

which is a small parameter (see eqs 8 and 9).

In the limit where  $\epsilon \ll 1$ , equation 22 simplifies considerably:

$$\phi_1 = \phi_2 \exp\left(-\frac{(1-\phi_2)^2}{2\epsilon}\right) \simeq 0 \quad (26)$$

Thus, as long as  $(1-\phi_2) \gg \epsilon^{1/2}$  (i.e.,  $\phi_2$  is not too close to unity), we can as well consider that  $\phi_1 = 0$  for the rest of our resolution to a very good approximation.

We can then immediately solve the diffusion equation 13, valid in region I, along with the boundary conditions 14. The solution can as usual be looked for as a function  $\phi(x, t) = f(u)$  of the reduced variable  $u = x/2\sqrt{D_s t}$ , and from eqs 23 and 26, we see that the boundary condition

on the moving boundary simply becomes  $\phi(-x_I^-, t) = f(-a) = 0$ . Solving the equation on  $f$ , we finally find the following concentration profile in region I, which involves the error function  $\text{erf } u = (2/\sqrt{\pi}) \int_0^u e^{-u^2} du$ , classical for semi-infinite media:

$$\phi(x, t) = \phi_0 - \frac{\phi_0}{1 - \text{erf } a} \left[ 1 + \text{erf} \left( \frac{x}{2\sqrt{D_s t}} \right) \right] \quad (\text{region I}) \quad (27)$$

We next turn to the determination of  $a$ , and thus to the determination of the position of the moving boundary at  $x = -x_I^-$ . Equation 19 will serve this purpose: with  $\phi_1 = 0$ , it simplifies to  $\dot{x}_I = -D_s \nabla \phi|_{x=-x_I^-}$ . Then, with the help of eq 23, which yields  $\dot{x}_I = a(D_s/t)^{1/2}$ , and of eq 27 which yields an expression of  $\nabla \phi|_{x=-x_I^-}$ , eq 19 finally brings the relation

$$\sqrt{\pi} a e^{a^2} (1 - \text{erf } a) = \phi_0 \quad (28)$$

This equation on  $a$  can be solved numerically to give the value of  $a$  as a function of the fundamental parameter  $\phi_0$  (which describes the initial state of the system). The result of the numerical resolution is shown in Figure 7.

The next step is to solve the diffusion equation 16 under the conditions 17, in order to find the concentration profile in region II. As equation 16 is a nonlinear equation without analytical solution (to the best of our knowledge), we will resort to numerical integration. We here again look for a solution  $\phi(x, t) = g(v)$  of the (new) reduced variable  $v = x/2\sqrt{D_f t}$ . The resulting differential equation on  $g$  turns out as:

$$\frac{d}{dv} \left( g(1 - g) \frac{dg}{dv} \right) = -2v \frac{dg}{dv} \quad (29)$$

and the boundary conditions of eq 17 translate to

$$(i) \quad \phi|_{x=-x_I^+} = g|_{v=-a\sqrt{\epsilon}} = \phi_2, \quad (ii) \quad \phi|_{x \rightarrow +\infty} = g|_{v \rightarrow +\infty} = 0 \quad (30)$$

It has to be noted that these boundary conditions, as such, are not sufficient to directly proceed to numerical integration, because the quantity  $\phi_2$  appearing there is *also* an unknown. We thus need a supplementary condition, which will be provided by the conservation equation of the B species (eq 20): using the definition of  $a$  (eq 23) and the definition of the reduced variable  $v$ , eq 20 can be rewritten as

$$\frac{dg}{dv} \Big|_{v=-a\sqrt{\epsilon}} = -\frac{2a\sqrt{\epsilon}}{\phi_2} \quad (31)$$

We have now enough equations to compute  $g(v)$  and the associated concentration profile in region II. We solve the set of equations 29–31 by a trial-and-error procedure: we choose an arbitrary value for the unknown  $\phi_2$ ; based on the corresponding initial conditions provided by eqs 30-(i) and 31, a numerical integration of eq 29 is performed; the obtained solution  $g$  is

then evaluated at infinity, and its value compared to zero (eq 30-(ii)); if different, the whole numerical procedure is resumed with a new chosen value for  $\phi_2$ , until the correct value of  $\phi_2$ , satisfying eq 30-(ii), is found. At the end of this process, we eventually obtain the actual profile of concentration  $\phi(x, t) = g(v)$  in region II, along with the value of  $\phi_2$  in our system. (See further down for the results.)

We are at this point in possession of the profiles  $\phi(x, t)$  in regions I, II and III, as well as of the numerical values of  $a$ ,  $\phi_1$ , and  $\phi_2$ . To complete our resolution, we still need to find the value of  $b$ , which is related to the position of the border between region II and III. This is easily performed numerically: by transposing the equation of motion for  $x_{\text{II}}$  established earlier (eq 18) in terms of the self-similar function  $g(v)$ , and applying the definition of  $b$  (eq 24), one obtains the relation

$$-2b = \frac{dg}{dv} \Big|_{v=b} \quad (32)$$

i.e.,  $b$  is a quantity such that the slope of  $g$  at  $v = b$  is equal to twice the value of  $b$  (with changed sign). The search for such a  $b$  can be carried on numerically with the function  $g$  calculated previously: the graph of  $b$  as a function of  $\phi_0$  can be found on Figure 7.

### 4.3 Presentation of results

We now present and comment on the results of the model, as obtained through the procedure described in the previous section.

As seen in eqs 23 and 24, the different “compartments” or regions composing the multiple interface are separated by diffusive fronts:  $x = -x_{\text{I}}(t) = -2a(D_{\text{st}})^{1/2}$  and  $x = x_{\text{II}}(t) = 2b(D_{\text{ft}})^{1/2}$ , with  $a$  and  $b$  are numerical parameters (see below for their values). The evolution in time of the concentration profiles of the different components is thus self-similar, and for this reason, it is useful to present them here in terms of the reduced variable  $u = x/2(D_{\text{st}})^{1/2}$ .

We remind our reader that there are two main physical parameters to our resolution:  $\phi_0$ , which represents the content in A of the initial A+A\* blend, and the small parameter  $\epsilon = 1/(2|\chi_{\text{AB}}|N) \ll 1$ , which is related to the strength of the attraction between A and B chains and the polymer chains length.

As these parameters were varied over a wide range of values ( $\phi_0$  between 0.1 and 0.9,  $\epsilon$  between  $10^{-5}$  and 0.1), it was observed that, remarkably enough, the (self-similar) diffusion profiles obtained retain the same aspect throughout; the main effect of varying the parameters is simply to *rescale* one or the other of the characteristic dimensions of the self-similar solution (i.e., stretch or shrink it in some region).

This generic self-similar diffusion profile for the A species is sketched in Figure 3 in terms of the reduced variable  $u$ . The fronts  $x = -x_{\text{I}}(t)$  and  $x = x_{\text{II}}(t)$  are respectively located at

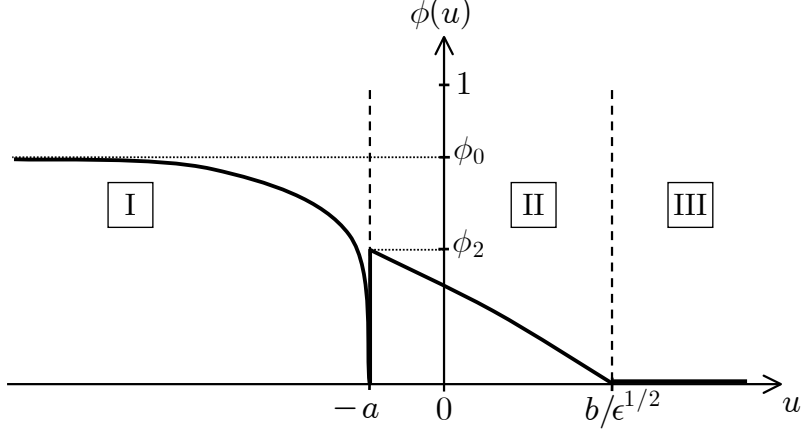


Figure 3: Sketch of the generic self-similar diffusion profile for species A: the volume fraction  $\phi$  has been drawn versus the reduced variable  $u = x/2\sqrt{D_s t}$ . The volume fractions used in the text,  $\phi_0$  and  $\phi_2$ , are also represented. In domain I (*i.e.* for  $u < -a$ ), the concentration profile is an error function; in domain II (*i.e.* for  $-a < u < b/\epsilon^{1/2}$ ), the profile is quasi-linear. In region III, A is absent.

$u = -a$  and  $u = b/\sqrt{\epsilon}$ . The profile in region I is given by an “error function”, typical of diffusion problems, and drops to zero at the approach of region II (since we proved that  $\phi_1 \simeq 0$  in practical cases). At the boundary between regions I and II (we neglect the thickness of the intermediate region IV), there is a discontinuous concentration jump from  $\phi = 0$  to  $\phi = \phi_2$ , and then the diffusion profile decreases smoothly until reaching zero at the border with region III. It should be emphasized as a very interesting feature of the solution that the amplitude  $\phi_2$  of this concentration jump remains constant in time and does not die away during the diffusion process.

We also note that, from an empirical point of view, the profile in region II does not have a very significant curvature; if needed, we might thus approximately regard it as a straight line.

As an illustration of the generic sketch of the diffusion profile described above, we have plotted in Figure 4 two actual profiles, computed numerically for different values of  $\phi_0$  (and same  $\epsilon$ ), which do show that, within some rescaling, the generic shape of Figure 3 is retained in both cases.

For completeness, we also give the corresponding generic self-similar profiles for the other mixture components in Figures 5 and 6. As reminded in Figure 3, the diffusion profile involves several characteristic quantities  $a$ ,  $b$ , and  $\phi_2$ , whose values we know consider in detail.

In Figures 7 and 8, we plot the variations of these quantities as functions of our model parameter  $\phi_0$ , *i.e.*,  $a(\phi_0)$ ,  $b(\phi_0)$ , and  $\phi_2(\phi_0)$ , at fixed  $\epsilon$  (*i.e.*, we work at given system chemistry, and change the initial composition of the mixture). It is observed that for  $0.1 \lesssim \phi_0 \lesssim 0.9$  (where

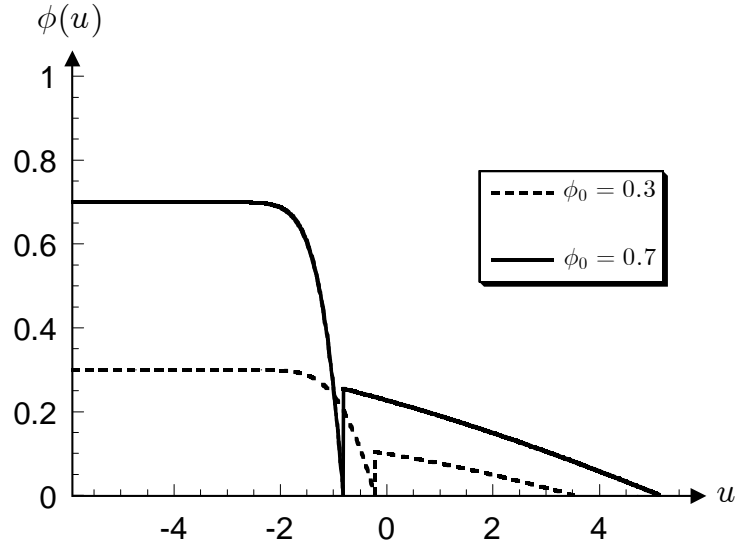


Figure 4: Numerical profiles for the volume fraction  $\phi(u)$  of the A species. The chain length and Flory parameter are  $N = 10^3$  and  $\chi_{AB} = 0.1$ , yielding  $\epsilon = 5 \cdot 10^{-3}$ . The solution  $\phi(u)$  has been represented for two values of the initial volume fraction of the A species in the A-A\* block:  $\phi_0 = 0.3$  and  $\phi_0 = 0.7$ .

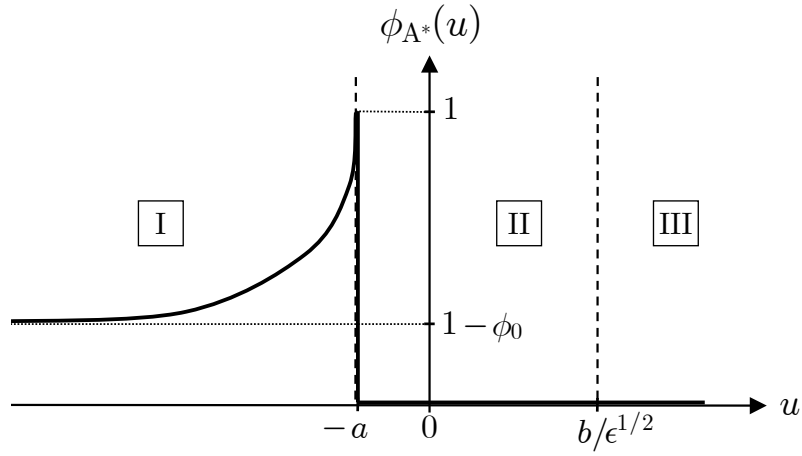


Figure 5: Sketch of the generic self-similar diffusion profile for the A\* species: the volume fraction  $\phi_{A^*}$  has been drawn versus the reduced variable  $u = x/2\sqrt{D_s t}$ . In region I,  $\phi_{A^*} = 1 - \phi$  and is thus given by a complementary error function. In the other regions, A\* is absent.

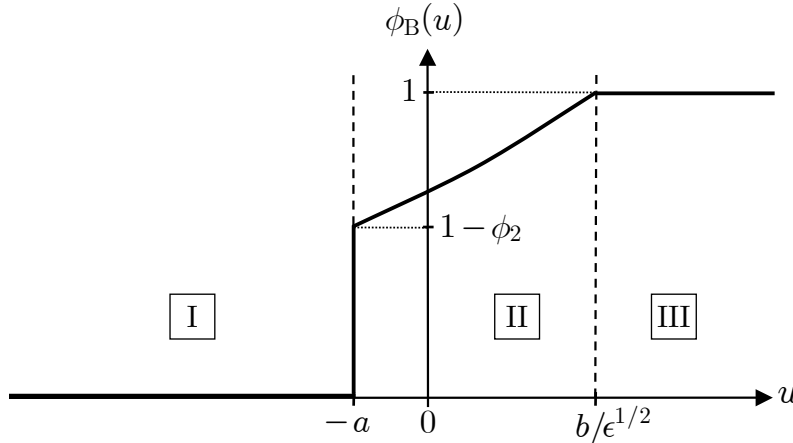


Figure 6: Sketch of the generic self-similar diffusion profile for the B species: the volume fraction  $\phi_B$  has been drawn versus the reduced variable  $u = x/2\sqrt{D_s t}$ . In region I, B is absent; in region II, the profile of B is the complement of A ( $\phi_B + \phi = 1$ ) and is quasi-linear; in region III, B is alone.

our resolution is valid), these quantities show a steady increase with  $\phi_0$ .

It is also possible to give rough analytical estimates of the dependence of  $a$ ,  $b$ , and  $\phi_2$  with respect to our other main parameter,  $\epsilon$ . The quantity  $a$  is given by the resolution of eq. 28, which involves only  $\phi_0$ ; thus we see that  $a$  has no functional dependence on  $\epsilon$  (at least in the regime  $\epsilon \ll 1$  considered in this article). Let us now estimate the dependencies of  $\phi_2$  and  $b$  on  $\epsilon$ : for that purpose, we will consider, in first approximation, that the concentration profile is linear in region II (see above). Writing as previously the solution  $\phi(x, t) = g(v)$  in terms of the reduced variable  $v = x/2(D_f t)^{1/2}$ , the (“constant”) value of the slope  $dg/dv$  is easily estimated: since  $g(v)$  goes from  $\phi_2$  at the left boundary of region II ( $v = -a\sqrt{\epsilon}$ ) to zero at the right boundary ( $v = b$ ), we have  $dg/dv \simeq -\phi_2/(b + a\sqrt{\epsilon}) \simeq -\phi_2/b$ . We then use this expression of the slope into eq 30-(i) and eq 31, and solve this set of two equations for  $b$  and  $\phi_2$ . This brings the following estimates:

$$b \simeq \left( \frac{a^2}{4} \epsilon \right)^{1/6}, \quad \phi_2 \simeq (2a^2 \epsilon)^{1/3} \quad (33)$$

In terms of scaling laws with respect to  $\epsilon$ , we thus have

$$b \sim \epsilon^{1/6}, \quad \phi_2 \sim \epsilon^{1/3}, \quad a \sim \epsilon^0 \quad (34)$$

(where the last equation is meant to recall that  $a$  has no dependence on  $\epsilon$ ).

Finally, we conclude the presentation of our results, by emphasizing one unusual and notable feature of our solution: as time goes on, region II, where A and B mix, grows in a very asymmetric

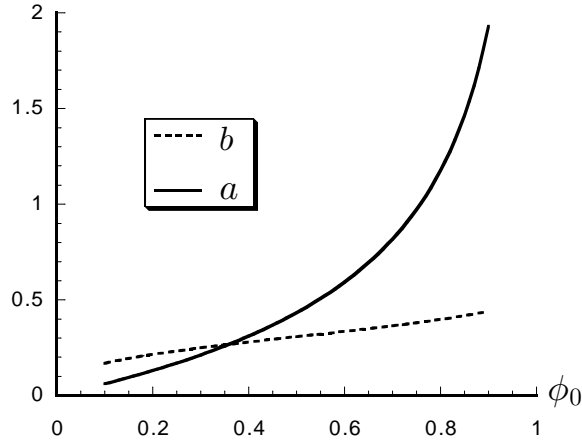


Figure 7: Values of the numerical factors  $a$  and  $b$ , which characterize the two moving boundaries  $x_I(t) = -2a(D_s t)^{1/2}$  and  $x_{II}(t) = 2b(D_f t)^{1/2}$ , plotted versus the initial volume fraction  $\phi_0$ . ( $\phi_0$  is ranging from 0.1 to 0.9 and  $\epsilon$  is fixed at  $5 \cdot 10^{-3}$ .)

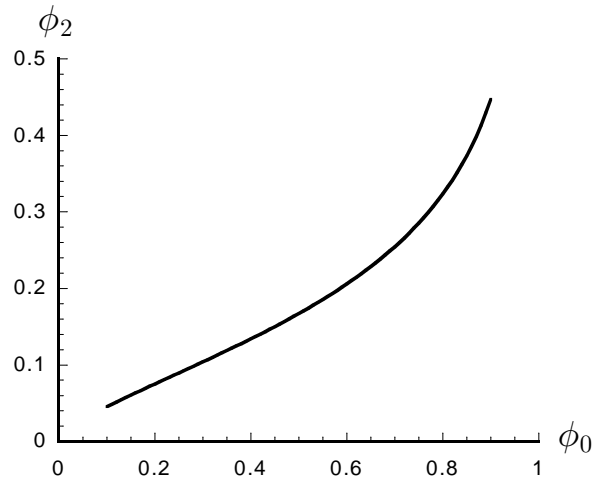


Figure 8: Plot of the quantity  $\phi_2$ , which corresponds to the amplitude of the concentration jump at the border between region I and II, versus the parameter  $\phi_0$ . ( $\phi_0$  is ranging from 0.1 to 0.9 and  $\epsilon$  is fixed at  $5 \cdot 10^{-3}$ .)

fashion, relatively to the position of the initial interface ( $x = 0$  at  $t = 0$ ); this is due to the fact that its two boundaries are of very different nature, with the right boundary  $x = x_{\text{II}}$  having a much faster diffusive motion than the left boundary  $x = -x_{\text{I}}$  (because  $D_{\text{f}} \gg D_{\text{s}}$ ). The ratio of these two boundaries' position is in fact independent of time and can be estimated as

$$\frac{x_{\text{I}}(t)}{x_{\text{II}}(t)} = \frac{a}{b} \left( \frac{D_{\text{s}}}{D_{\text{f}}} \right)^{1/2} \sim \epsilon^{-1/6} \epsilon^{1/2} \sim \epsilon^{1/3} \quad (35)$$

The sluggishness of the motion of  $x_{\text{I}}$  relatively to  $x_{\text{II}}$  thus becomes more pronounced as  $\epsilon$  becomes smaller, i.e., if the attraction between A and B is made stronger or if the polymer chains length is increased (see eq 25).

We have now completed the resolution of the dynamics of our three-species system, and have presented the results that were obtained.

## 5 Concluding remarks

In this article, we studied the evolution of the interface between two polymer melts, in a specific case where three species of strongly contrasting chemical affinities were involved. It was found that, due to the simultaneous presence of entropy and enthalpy-driven diffusion processes, the dynamics at the interface is unusual (with a very asymmetric growth of the mixing layer), and that moreover, the interface shows a peculiar spatial structuration in three distinct layers of different chemical compositions.

Let us now close with some remarks. Obtaining a triad of polymers with chemical properties such as specified in eqs 9-11 is certainly a difficult task. One potential way could be the following: (i) having A and B strongly attracted to each other through the existence of hydrogen bonds, (ii) having  $A^*$  a very slightly modified variant of A, where hydrogen bonding to B becomes unavailable; then between A and B, van der Waals attractions will dominate, leading to repulsion, while hopefully A and  $A^*$  will remain similar enough and roughly indifferent to each other.

The case which has been described and studied in this article is, as has been argued in the Introduction, only one limiting situation in a vast range of multiple species interfaces in polymer systems, and has been selected for the strong opposing tendencies in the chemical affinities of the involved polymers. Our hope is however to demonstrate on this example the richness of multiple-species interfaces, where many other such “selected cases” would be worth investigating and studying for their peculiar structure and dynamics.

From the application point of view, the ability to spontaneously form (at least in some cases) a *multi-layered interface* between two polymer blocks, might lead to interesting perspectives in the design of multilayer polymer films<sup>36</sup>— which are widely used for product packaging, for instance.

Whereas conventional technology includes processes like coating, lamination, or coextrusion to form multilayered films, here the layering appears by means of a purely diffusional process. The chemical composition and the spatial organization of the layering could be controlled through an appropriate choice of chemical affinities between the different species in interaction, and once the desired result is attained, the system could be quenched to freeze the diffusion process (e.g., for prescribed layer thicknesses).

## Acknowledgements

We are very grateful to F. Brochard-Wyart, F. Chevy, C. Creton and M. Winnik for useful discussions.

## Appendix. Derivation of governing equations

In this Appendix, we give a detailed derivation of some of the governing equations presented in section 4.1.

### Equation of motion for $x_{\text{II}}(t)$

Equation 18 is obtained as follows. By definition,  $x_{\text{II}}(t)$  is the point such that, at any time  $t$ ,  $\phi(x_{\text{II}}(t), t) = 0$ . Since  $\phi$  is a constant over time at that point, we also have that the total time derivative at that (moving) point,  $d\phi/dt|_{x=x_{\text{II}}}$ , must be zero:

$$\frac{d\phi}{dt} \bigg|_{x=x_{\text{II}}} = \dot{\phi}|_{x=x_{\text{II}}} + \dot{x}_{\text{II}} \cdot \nabla \phi|_{x=x_{\text{II}}} = 0$$

Furthermore, using the diffusion equation 16 and  $\phi|_{x=x_{\text{II}}} = 0$ , another expression for  $\dot{\phi}$  is easily obtained:

$$\dot{\phi}|_{x=x_{\text{II}}} = D_f (\nabla \phi|_{x=x_{\text{II}}})^2$$

Substitution of the latter equation into the former yields equation 18.

### Conservation of the B species

We now show how relation 20 derives from the conservation of the B species.

As a little reflection from the consideration of Figures 1 and 2 can make clear, the conservation of the B species writes as follows:

$$\int_{-x_{\text{I}}(t)}^{x_{\text{II}}(t)} \phi_B dx = x_{\text{II}}(t) \cdot 1 \quad (36)$$

This expression simply states that, when considering the situation at a certain time  $t > 0$ , all the initial B material which was comprised between  $x = 0$  and the present position  $x = x_{\text{II}}(t)$  (a quantity equal to  $x_{\text{II}} \cdot 1$  since the initial volume fraction of B was one) has been redistributed by virtue of the interdiffusion process all over region II (hence the term  $\int_{-x_{\text{I}}(t)}^{x_{\text{II}}(t)} \phi_B \, dx$  on the left-hand side). Using  $\phi_B = 1 - \phi$ , one then obtains

$$\int_{-x_{\text{I}}(t)}^{x_{\text{II}}(t)} \phi \, dx = x_{\text{I}}(t) \quad (37)$$

Differentiating eq 37 once with respect to time, using eq 16 and  $\phi(x_{\text{II}}) \equiv 0$ , one obtains a local version of this integral equation:  $\dot{x}_{\text{I}} = -\phi_2 \cdot D_f \nabla \phi|_{x=-x_{\text{I}}^+}$ , which is exactly equation 20.

### Conservation of the A species

We now derive equation 19 from the conservation of species A. The conservation equation for A has the form

$$\int_{-x_{\text{I}}(t)}^{x_{\text{II}}(t)} \phi \, dx = \phi_0 x_{\text{I}}(t) + \int_{-\infty}^{-x_{\text{II}}(t)} (\phi_0 - \phi) \, dx \quad (38)$$

This expression has the following meaning: at time  $t$ , the A material enclosed in region II ( $\int_{x=-x_{\text{I}}}^{x=x_{\text{II}}} \phi \, dx$ ) comes from the material which was initially present between  $x = -x_{\text{I}}$  and  $x = 0$  at volume fraction  $\phi_0$ , plus the amount that has diffused from region I ( $\int_{-\infty}^{-x_{\text{II}}} (\phi_0 - \phi) \, dx$ ). Using eq 37 into eq 38, then differentiating with time and substituting with the diffusion eq 13, one finally obtains the following local version for the conservation of the A species:  $\dot{x}_{\text{I}} = -(1 - \phi_1)^{-1} \cdot D_s \nabla \phi|_{x=-x_{\text{I}}^-}$ , which is precisely equation 19.

### Relation between $\phi_1$ and $\phi_2$

We now explain how one obtains equation 22 from 21.

Using classical formulae<sup>1,5,32</sup> to compute the chemical potential of A, one obtains the expression

$$\mu_A = kT [\log \phi + \chi N(1 - \phi)^2] \quad (39)$$

This expression for  $\mu_A$  holds for blends made of *two* polymeric species, characterized by a Flory parameter  $\chi$  (and under the assumption that these species have the same chain length  $N$ ). Thus, eq 39 should not be used to compute  $\mu_A$  within region IV, where three component coexist; but it can indeed be used right at the borders with regions I on one side and region II on the other — there one of the components drops to zero concentration, thereby leaving us with two species only.

On the left border of region IV ( $x = -x_I^-$ ), we only have the two species A and A\* (since  $\phi_B \rightarrow 0$ ), and accordingly, we can apply formula 39 with  $\chi = \chi_{AA^*} \simeq 0$ , which yields

$$\frac{\mu_A(-x_I^-)}{kT} = \log \phi_1$$

Similarly, on the right border ( $x = -x_I^+$ ), only A and B coexist, and we find

$$\frac{\mu_A(-x_I^+)}{kT} = \log \phi_2 + \chi_{AB} N(1 - \phi_2)^2$$

Writing the equality between the above two expressions of the chemical potential (as required by eq 21) finally yields the governing equation 22.

## References

- [1] Jones, R. A. L; Richards, R. W. *Polymers at Surfaces and Interfaces*; Cambridge University Press: Cambridge, 1999)
- [2] Wool, R. P. *Polymer Interfaces: Structure and Strength*; Hanser Publications: Cincinnati, 1995.
- [3] *Physics of Polymer Surfaces and Interfaces*; Sanchez, I. C., Fitzpatrick, L. E., Eds.; Butterworth-Heinemann: London, 1992.
- [4] *Polymer Surfaces and Interfaces III*; Richards, R. W., Peace, S. K., Eds.; Wiley and Sons: New York, 1999.
- [5] de Gennes, P.-G. *Scaling Concepts in Polymer Physics*; Cornell University Press: Ithaca (NY), 1979.
- [6] Jabbari, E.; Peppas, N. A. *Polymer* **1995**, *36*, 575.
- [7] The free energy of mixing of an A/B polymer melt is rather well described by the simple Flory-Huggins approach, which is a tractable, two-species polymeric version of a lattice gas model. The two first terms in the right-hand side of the expression 6 give the entropic contribution of  $f$ , which is assumed to take a simple ideal gas form. The last term stands for the enthalpy of mixing, estimated within a mean-field picture. See: Flory, P., *Principles of Polymer Chemistry*; Cornell University Press: Ithaca (NY), 1971, Chap. XII. Huggins, M. *J. Am. Chem. Soc.* **1942**, *64*, 1712.
- [8] Bates, F. S.; Wignall, G. D. *Phys. Rev. Lett.* **1986**, *57*, 1429.

[9] (a) Helfand, E. *Polymer Compatibility and Incompatibility*; K. Solc. Chur: Harwood, 1982.  
 (b) Helfand, E.; Tagami, Y. *J. Polym. Sci.* **1971**, *B9*, 741. (c) Idem. *J. Chem. Phys.* **1971**, *56*, 3592. (d) Idem. *J. Chem. Phys.* **1972**, *57*, 1812.

[10] Crank, J. *The Mathematics of Diffusion*; Clarendon Press: Oxford, 1975.

[11] de Gennes, P.-G. *C. R. Acad. Sci. Paris, Sér. II* **1980**, *291*, 219.

[12] Prager, S.; Tirell, M. *J. Chem. Phys.* **1981**, *75*, 5194.

[13] Kim, Y. H.; Wool, R. P. *Macromolecules* **1983**, *16*, 1115.

[14] Adolf, D.; Tirell, M.; Prager, S. *J. Polym. Sci.: Polym. Phys. Ed.* **1985**, *23*, 413.

[15] Zhang, H.; Wool, R. P. *Macromolecules* **1989**, *22*, 3018.

[16] Brochard, F.; de Gennes, P.-G. *Europhys. Lett.* **1986**, *1*, 221.

[17] Brochard-Wyart, F.; de Gennes, P.-G. *Makromol. Chem. Macromol. Symp.* **1990**, *40*, 167.

[18] Shibayama, M.; Yang, H.; Stein, R. S.; Han, C. C. *Macromolecules* **1985**, *18*, 2179.

[19] (a) Onsager, L. *Ann. NY Acad. Sci.* **1933**, *34*, 241. (b) Onsager, L. *Phys. Rev.* **1931**, *37*, 405.

[20] de Gennes, P.-G. *J. Chem. Phys.* **1980**, *72*, 4756.

[21] Brochard, F.; Jouffroy, J.; Levinson, P. *Macromolecules* **1983**, *16*, 1638.

[22] Brochard, F.; Jouffroy, J.; Levinson, P. *J. Phys. Lett.* **1983**, *44*, 455.

[23] Kramer, E. J.; Green, P.; Palstrøm, C. J. *Polymer* **1984**, *25*, 473.

[24] Sillescu, H. *Makromol. Chem. Rapid Comm.* **1987**, *8*, 393.

[25] (a) Klein, J. *Nature* **1978**, *271*, 143. (b) Klein, J.; Briscoe, B. J. *Proc. Roy. Soc. London A* **1979**, *365*, 53.

[26] Gilmore, P. T.; Falabella, R.; Lawrence, R. L. *Macromolecules* **1980**, *13*, 880.

[27] Seggern, J. V.; Klotz, S.; Cantow, H. J. *Macromolecules* **1989**, *22*, 3828.

[28] Jordan, E. A.; Ball, R. C.; Donald, A. M.; Fettes, L. J.; Jones, R. A. L.; Klein, J. *Macromolecules* **1988**, *21*, 235.

- [29] (a) Brochard-Wyart, F. Proc. Toyota Conf., *Stud. Polym. Sci.* **1988**, *2*, 249. (b) Brochard-Wyart, F. *C. R. Acad. Sci. Paris* **1987**, *305*, 657.
- [30] In the regime of entangled polymer chains, Brochard's amended approach gives exactly the same expressions for the diffusion coefficients as in the model of Kramer's et al. It should be noted, however, that a discrepancy remains in the case of short, non-entangled chains.
- [31] Note that the last boundary condition in eq 17 resides within region III, not II; this is admissible, because the diffusion equation 16 is indeed valid in region III as well as in region II. The boundary conditions stated here in fact automatically generate a solution which vanishes to zero at some *finite* position  $x = x_{\text{II}}(t)$  and afterwards keeps that value for all  $x > x_{\text{II}}$ : they thereby naturally give birth to our region III (defined earlier as the region where  $\phi = 0$ ) without the need of further constraints to be imposed, and are the correct ones to use.
- [32] Doi, M. *Introduction to Polymer Physics*; Oxford University Press: Oxford, 1996.
- [33] Russel, T. P.; Deline, V. R. *Nature* **1993**, *365*, 235.
- [34] de Gennes, P.-G. *C. R. Acad. Sci. Paris, Sér. II* **1981**, *292*, 1505.
- [35] de Gennes P.-G. *C. R. Acad. Sci. Paris, Sér. II* **1989**, *308*, 13.
- [36] Briston, J. H. In *Encyclopedia of Advanced Materials*, vol. 2; Bloor, D., Brook, R. J., Flemings, M. C., Mahajan, S., Eds.; Pergamon Press: New York, 1994.